Eur. J. Mech. B - Fluids 19 (2000) 653–672

S0997-7546(00)00125-4/FLA

The near-wall layer beneath a moderately converging three-dimensional turbulent separated and reattaching flow

J. Ralph Hardman *, Philip E. Hancock [1]

School of Mechanical and Materials Engineering, University of Surrey, Guildford, Surrey GU2 5XH, UK

(Received 1 April 1999; revised 17 January 2000; accepted 20 January 2000)

Abstract – Pulsed-wire mean velocity and surface shear stress measurements have been made in a three-dimensional separation bubble in which there is a mild lateral convergence, bounded by side regions of spanwise invariance. Even though the convergence is mild the bubble parameters change considerably with lateral position. Velocity measurements near the surface were made with a special through-wall pulsed-wire probe. The cross-flow layer is substantially thicker than the reverse-flow layer even in the invariant region. Cross-flow and reverse-flow velocity profiles are each remarkably close in shape, though probably not exactly self similar. Surface shear stresses in the cross- and reverse-flow directions conform to local scalings and Reynolds-number dependences based on thickness and 'external' velocity. These scalings also apply (quantitatively) downstream of and, it appears, through attachment. The surface shear stress in the cross-flow direction is higher than the streamwise stress, consistent with a distinctly fuller mean velocity profile. There is a striking comparability with three-dimensional boundary layers once the flow directions are transposed, the cross flow taking the part of the primary flow, and the reverse flow the secondary flow. © 2000 Éditions scientifiques et médicales Elsevier SAS

turbulent separated flow / near-wall layer

1. Introduction

Studies of turbulent separated flows largely fall into two broad categories – those in which the mean flow is nominally two-dimensional and coplanar, and those where the mean flow is highly three-dimensional and therefore considerably more complex. For the latter comparatively little is known regarding the turbulence structure and, moreover, there is no systematic link between the 'simple' case of the former – studied for obvious reasons – and the more general. In general all nine rates of mean strain are present, which is one of the complicating features of three-dimensional separated flows, while in precisely two-dimensional coplanar flows there can be no more than four, of course, two of which are linked. Extra rates of strain are well known to have a large effect on turbulence structure.

An obvious extension of the two-dimensional, coplanar flow is the swept flow in which the effect of sweeping the separation line is to add a cross flow, making the flow no longer coplanar, as in the studies of Sutton et al. [1] and Fernholz et al. [2], for example. Ideally, this flow, as with its unswept counter part, is such that it is genuinely two-dimensional and free from end effects. That is, the flow is invariant with 'spanwise' position (where the term 'spanwise' is used in the aeronautical sense to denote lateral position). Spanwise-invariant flows are of course themselves special cases, of which the unswept flow is one particular instance. In these, in topological terms, the velocity components lying in a plane perpendicular to the direction of invariance (z, say) define pseudo streamlines in this plane, where these pseudo streamlines must be as in two-dimensional coplanar flows (because $\partial W/\partial z$ is zero, where W is the velocity in the z-direction). Therefore, the separating

* Present address: Computational Dynamics (Germany), Dürrenhofstrasse 4, 90402 Nürnberg, Germany
[1] Correspondence and reprints; e-mail: P.Hancock@surrey.ac.uk

streamline must also be an attaching streamline, and can therefore properly be called a 're'attaching streamline. Streamlines beneath the reattaching streamline must remain within the bubble, and the pseudo streamlines must form closed streamlines, the true streamlines lying on cylindrical surfaces. More generally, however, the flow will locally converge or diverge, and the separating streamlines will lie above or below the attaching streamlines, respectively, as illustrated in *figure 1*. This is true even on planes of symmetry, although this point is sometimes overlooked. Here, therefore, although the flow itself is a reattaching flow, we use the term attachment, rather than reattachment, to refer to the attaching streamline.

Measurements of the near-wall layer beneath nominally two-dimensional coplanar flows have been made by Simpson [3], Adams and Johnston [4], Dianat and Castro [5], and Devenport and Sutton [6]. This layer, defined as the region between the surface and the position of maximum reverse-flow velocity, is thin compared with height of the separation bubble, and exhibits 'laminar-like' features rather than anything resembling a logarithmic law, which in any case would not be expected (although it is very widely assumed in CFD). The velocity profile is at least approximately self-similar, and the shear stress varies with Reynolds number in much the same way as in a laminar boundary layer (though the magnitude is larger). Simpson suggests an analytic form for the velocity profile $U(y)$, namely $U/U_N = A[y/N - \ln(y/N) - 1] - 1$, though it appears to have escaped attention of a number of investigators that the coefficient A should in fact be multiplied by the ratio of the friction velocity to the maximum reverse-flow velocity, u_τ/U_N, for the form to be consistent with viscous scaling near the surface. N is the thickness of the layer as defined by the point where $U = U_N$, later denoted by $\delta_{U'}$ and U'_δ in this paper. Devenport and Sutton [6] make an allowance for A to vary but on a different analytical basis. Attention has been directed exclusively it would seem to the near-wall layer upstream of attachment, although there is a comparably thin layer developing on the downstream side. Indeed, the present results (see also Hancock [7]) show these two layers to behave in the same manner.

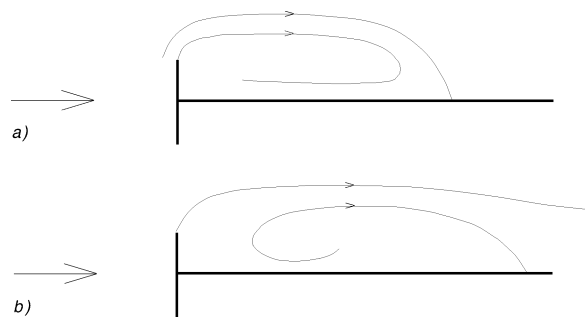

Figure 1. Normal flat plate ('fence') and splitter plate, and 'sketch' of separating and attaching streamlines: (a) diverging (z-direction) flow; (b) converging flow.

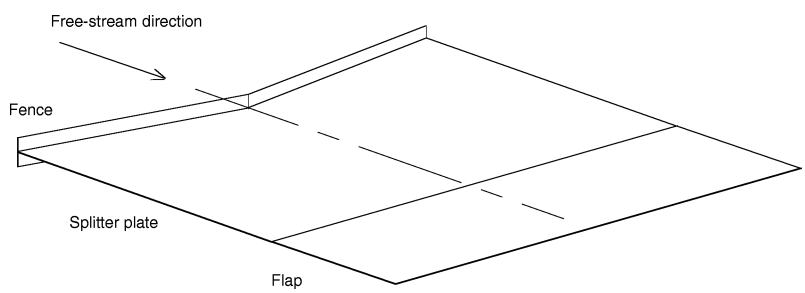

Figure 2. Flow rig for bubble downstream of v-shaped separation line. Drawing approximately to scale, except height of fence is exaggerated (by factor of 5).

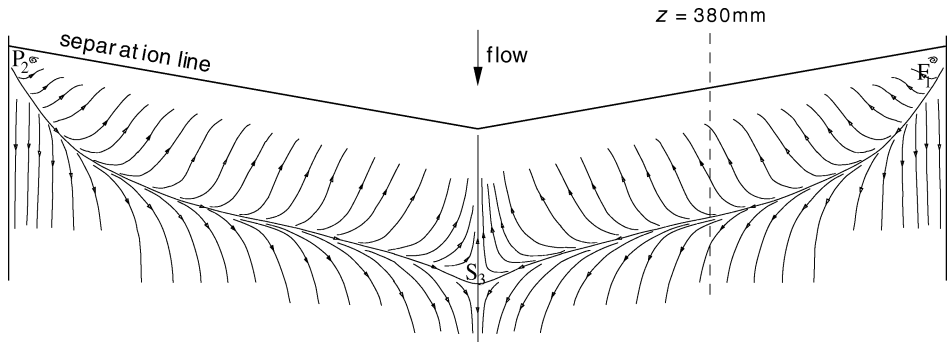

Figure 3. Surface streamlines on splitter plate. View from above.

The present flow was generated by means of a doubly-swept separation line, formed by a normal flat plate mounted on the front of a horizontal splitter plate as, illustrated in *figures 2* and *3*. The degree of three-dimensionality is 'moderate' in the sense that the cross flow velocity is substantially less than the free-stream velocity. The flow was set up with the intention that it should be wide enough for the flows at the sides of the central region to be spanwise-invariant, free from the influences of either the central or wind-tunnel-wall regions. Although this was not fully achieved, and the flow there was not precisely spanwise-invariant, the consequences turn out to be of no significance in the present context, as will be seen later. It is perhaps worth commenting that very few of the detailed studies on nominally two-dimensional (coplanar) separated flows have in fact been made in flows of adequate width to be free of significant end effects (see, e.g., Hancock and McCluskey, [8]; Hancock, [7]). Even though the present case is regarded as mildly three-dimensional, generated as it is by side flows of sweep $\pm 10°$, the effect on the bubble near the central plane is to almost double the height of the shear layer at attachment. A summary of the outer flow is given by Hardman and Hancock [9]. A convenient feature of the present flow (which cannot be assumed a priori) is that all the evidence shows it to be symmetric about the centre plane. Such a feature will be convenient also in the context of computational studies, where another purpose of spanwise-invariant side regions is that the 'inflow' conditions should then be well defined, at least in principle. Measurements were also made in a two-dimensional, coplanar 'reference' flow, downstream of an unswept separation line.

It is to be anticipated that there should be at least some qualitative comparability between the present near-wall layer and that of three-dimensional boundary layers. Indeed, McCluskey and Hancock found that in their spanwise invariant flow the velocity vector followed a velocity triangle form (Johnston, [10]), even in the reverse-flow region, with the flow near the surface appearing to exhibit a locally coplanar behaviour, though their velocity measurements did not reach into the near-wall layer. As will be seen later, although there is a link with three-dimensional boundary layers it is not as might be expected.

The velocity and surface shear stress measurements presented here, which appear to be the first of their kind in this type of flow, were made by means of pulsed-wire anemometry, with the components of velocity parallel to and near the surface measured by means of a special 'through-wall' probe. Only the mean flow features are presented here; details concerning the fluctuating velocities and shear stresses will be given in another paper. Further details are given by Hardman [11].

2. Flow rig and measurement techniques

As has been mentioned already, the separation bubble was generated behind a vertical flat plate (or 'fence'), made in two parts, mounted on the front of a horizontal, v-shaped splitter plate, as illustrated in *figure 2*. The

sharp tips of the normal plates were at a fence height, h_f, of 10.0 mm above and beneath the splitter plate surfaces, where the splitter plate thickness and length were 3.0 mm and 1 m (at the sides), respectively. The model was supported in the centre of the 1.53 m-wide by 0.5 m-high working section of the 'B' wind tunnel of the School of Mechanical and Materials Engineering, by means of slender legs. A flap of length 0.5 m at the downstream edge of the splitter plate was inclined slightly to make the bubbles above and below the splitter plate equal in size. The working section and contraction had been designed specifically for the present task in order to give more than adequate flow width both sides of the centre line, though with a smaller fence and hence smaller bubble size. However, the larger fence was necessary in order to reduce the effect of probe size. For the measurements in the unswept flow the v-shaped splitter plate was replaced by a rectangular plate. h_f was also 10.0 mm. The free-stream velocity in the upstream flow was 5.8 m/s throughout, giving a Reynolds number based on h_f of 3900.

The pulsed-wire technique is specially designed for measurements in turbulent separated flows, which unlike hot-wire anemometry for example, is able to distinguish fluctuating changes in flow direction. The velocity was measured by means of two types of 'miniature' pulsed wire probe. One of these, the 'field' probe, was held from above the bubble by means of a five-component, servo-driven traverse mechanism mounted above the roof of the wind tunnel. This probe had pulsed and sensor wire lengths of about 6 mm, where the sensor wires were about 0.7 mm from the pulsed wire and offset by about 25° to avoid the effect of the wake of one on the other during calibration. The diameters of the pulsed and sensor wires were 9 μm and 2.5 μm. The probe head was mounted on an especially slender support body which increased from 2 mm to 4 mm in diameter over its length of 200 mm, a long thin body being found necessary in order to keep interference effects to acceptably small levels, deemed to be satisfied if the reduction in attachment length was not more than 3% when the probe was present. It appears that the sensitivity to interference effects may have been underestimated in several previous studies.

The 'through wall' probe head was of similar size and proportions, but was mounted at the end of a special mechanism in which the height was controlled by a micrometer head, to an accuracy of 0.1 mm when allowing for uncertainty in the height of the pulsed wire. The arrangement, which is similar to that used by Castro and Dianat, and that recommended by Schober et al. [12], was supported in a special plug held in one of several streamwise slots in the splitter plate surface. The mechanism beneath the surface of the splitter plate was small enough for the interference it generated to have had negligible effect on the flow above the splitter plate. The remainder of this slot and the other slots were filled with plugs to provide a smooth leak-proof surface. The slots were at the lateral positions, z, of $-40, 0, 40, 80, 120, 200$ and 380 mm, where the last position was in the (nominally) spanwise-invariant region, and the first and third stations were used to confirm symmetry of the flow about the centre plane.

Both the field probe and the through-wall probe were calibrated against a Pitot-static reference probe (mounted in the upstream flow), with the calibration fitted by a polynomial of the form $U = A(1/T) + B(1/T)^3$, where T is the measured time of flight. This gave a very good fit except at the low velocity end of the through-wall probe calibration. The measurements in this range were corrected afterwards by means of a modified calibration

$$U = A(1/T) + B(1/T)^2 + C(1/T)^3, \tag{1}$$

fitted to the original calibration data, and an assumed form for the histogram of the fluctuations. The velocity measurements quoted here are accurate to within about $\pm 1\%$ of the reference velocity, U_{ref}. It was important that the error should be of this size or smaller for the present measurements because the cross flow velocity does not exceed about $0.17U_{ref}$, leading to an error in W of between zero and $\pm 12\%$ of U_{ref} if W is measured by the single difference between two orientations. In principle the measurement of W requires only two orientations of the pulsed-wire probe (for example 0° and 45°, or −45° and +45°, where the angle is the direction between

the normal of the probe head plane and the free-stream direction). In practice, as here, it is better to use several angles and obtain the mean and higher order moments from least-squares fits.

The through-wall probe was not calibrated for the effect of velocity gradient (see Schober et al., [12]) as this was beyond the scope of this initial investigation; as it turned out that effect is small enough to be ignored in the present context. The yaw response of the field probe was in excess of $\pm 80°$, and the pitch response, tested to $\pm 70°$, will have been equally large. Slight geometrical differences meant that the yaw range for the through-wall probe was less, but in excess of $\pm 70°$. Measurements were made at five or more probe angles about the mean flow direction. The errors in W should therefore be significantly less than $\pm 12\%$ of U_{ref}. Indeed, measurements on the centre line (where the variation in U is also the largest) show an error in W within about $\pm 2\%$ of U_{ref}, and the scatter in all the other profiles of W also falls within this band. The fact that the flow was (from self-consistency) closely symmetrical about the centre-plane meant that symmetry could be used to confirm probe alignment in the $U - W$ plane to within about $\pm 1°$. The errors arising from imperfect cosinal yaw response are small enough to neglect.

The pulsed-wire wall shear stress probe was calibrated against a Preston tube in a zero-pressure-gradient turbulent boundary layer (using Patel's [13] calibration), and fitted to the formally correct average of the calibration polynomial which was identical in form to that given by the right-hand side of equation (1). At least four probe angles were used in order to obtain the mean shear stress components and also the mean squares of the fluctuations of shear stress. The yaw response was cosinal to in excess of $\pm 85°$.

Surface streamlines were observed by means of fine titanium particles in paraffin oil, and from the ink-dot method of Langston and Boyle [14].

3. Results and discussion

As already mentioned, the surface streamlines on the splitter plate are shown in *figure 3*. The streamwise distance to the attachment, X_A, as inferred from flow visualisation and surface shear stress measurements is given in *table I*. Two axes systems will be used; see *figure 4*. In one, the 'fence axes', appropriate to the spanwise-invariant flow, x' is taken as the perpendicular distance from the separation line, and z' is taken parallel to the separation line, with the positive sense away from the centre, and with an arbitrary origin. In the other, the 'wind tunnel axes', z is taken from the symmetry plane and x is taken in the free-stream direction, with the origin at the separation line. In both sets y is the distance above the splitter plate surface. In the first set the velocity components in the x'- and z'-directions are, respectively, U' and W', and those in the x- and z-directions are U and W. These two pairs of velocities are related by

$$U = U'\cos(\theta) - W'\sin(\theta) \quad \text{and} \quad W = U'\sin(\theta) + W'\cos(\theta), \tag{2}$$

where θ is the sweep angle. X_A is the distance to attachment in the $x - z$ axes, and X'_A is the distance in $x' - z'$ axes (where in the spanwise-invariant region $x/X_A = x'/X'_A$). The surface shear stress components and related coefficients are similarly distinguished. For the spanwise-invariant flows the reference velocities U_0 and W_0 are employed, where $U_0 = U_{ref}\cos(10°)$ and $W_0 = U_{ref}\sin(10°)$, as shown in *figure 4*.

Table I. Distance to attachment, X_A, as a function of z.

z/(mm)	0	40	80	120	200	380
X_A/h_f	26	24.5	23.5	23	22	21

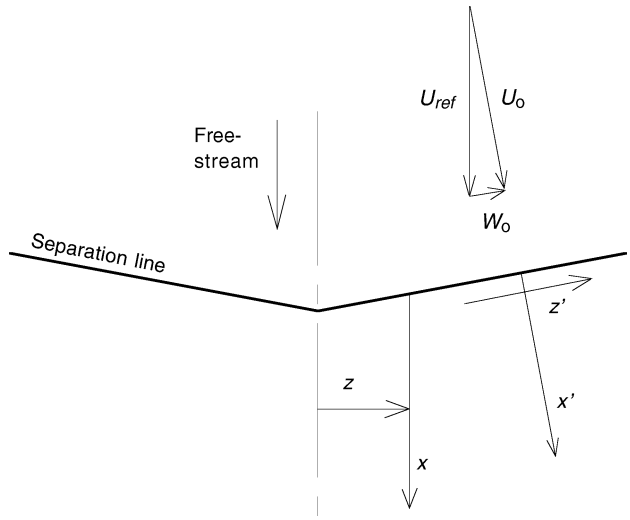

Figure 4. Coordinate axes.

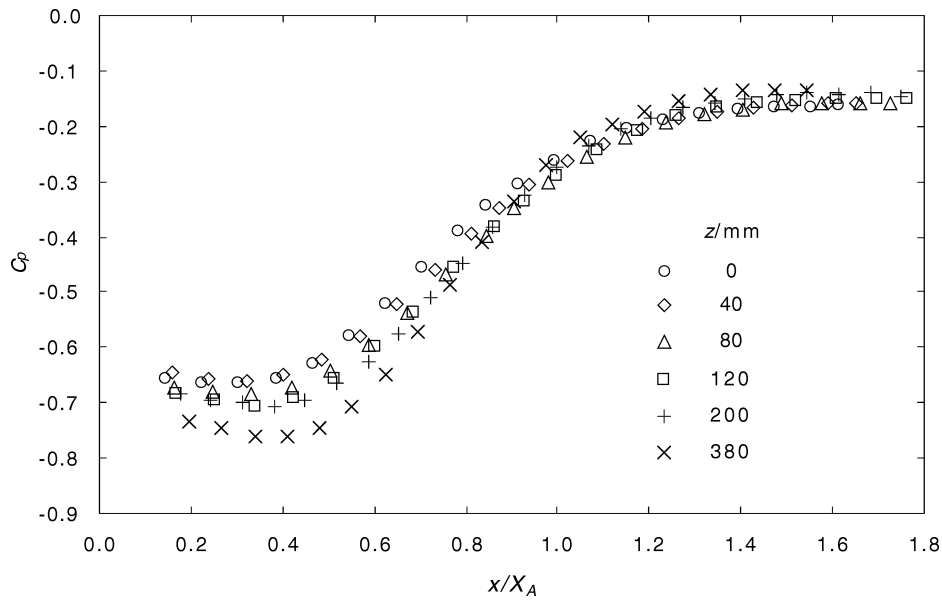

Figure 5. C_p as a function of x/X_A and z.

The pressure distributions at the six lateral stations are shown in *figure 5*, with x normalised by the local distance to attachment, X_A. Not unexpectedly, the pressure is less negative in the central region, and changes fairly slowly with z.

The results are presented in two stages, the first covering the nominally spanwise-invariant flow ($z =$ 380 mm), and the second covering the central region.

3.1. Spanwise-invariant flow

The surface shear stresses, $\tau_{x'}$ and $\tau_{z'}$ are shown in *figure 6*, normalised by $\rho U_0^2/2$. The figure also shows the magnitude of the shear stress, normalised in the same way. $\tau_{x'}$ is very comparable with the measurements of Hancock [15] once the difference in normalising velocity and the dependence on Reynolds number are taken into account, the slightly higher level here being consistent with the effect of aspect ratio (Hancock, [7]).

For moderate cross flow there is very little change in the velocity in the x'-direction with sweep angle, once normalised on U_0. That is, U'/U_0 is close to that in a two-dimensional coplanar flow, as shown by McCluskey and Hancock [8]. (U'/U_0 is also fairly close to that measured by Ruderich and Fernholz [16] and Castro and Haque [17], although as discussed by Hancock, their measurements were not free of end effects.) At the present small sweep angle there is also very little difference between U'/U_0 and U/U_{ref}. There is therefore no need to present profiles of U'/U_0 here, though some examples of U/U_{ref} are given later (section 3.2). The cross flow velocity W', normalised by W_0 is given in *figure 7(a)*. The same data is also given in *figure 7(b)* but referred to wind tunnel axes – that is, as W (and normalised by U_{ref}), the change of shape arising from the contribution from U' – see equation (2). The dip in W' at $x'/X'_A = 0.24$ seen at about $y/h_f = 2.6$, and also visible in *figure 7(b)* by the early rise in W, is a curious consequence of the flow not being completely free from end effects, as can be inferred from measurements nearer the centre plane; there is no reason to believe the dip to be spurious.

A polar presentation of velocity, that is of W as a function of U, is given in *figure 8*, where wind tunnel axes have been used. In this form of presentation, frequently employed in studies of three-dimensional boundary layers, y is an implicit variable; y is zero at the origin and increases with distance along each curve. The 'shape' is identical if W' is given against U' because the velocities in the two sets of axes are related by the linear transformation for the rotation of axes, as given earlier by equation (2). This figure also shows the limiting direction inferred from the wall shear stress, and confirms the view that very near the surface the flow is locally coplanar. A distinctive feature that was not observed by McCluskey and Hancock is that at the outer edge W

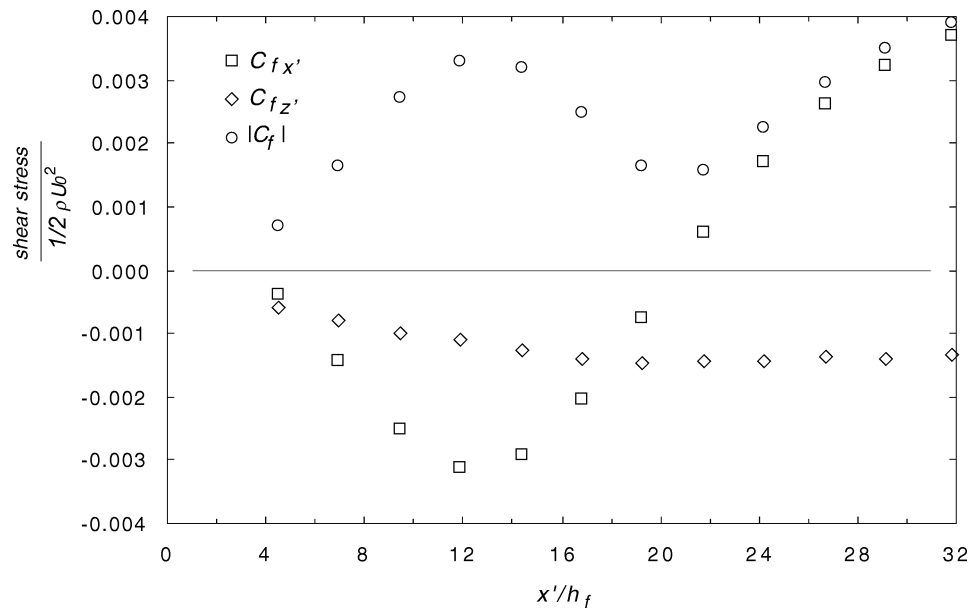

Figure 6. Shear stresses, $\tau_{x'}$ and $\tau_{z'}$, and the shear stress magnitude, τ, normalised by U_0, at $z = 380$ mm.

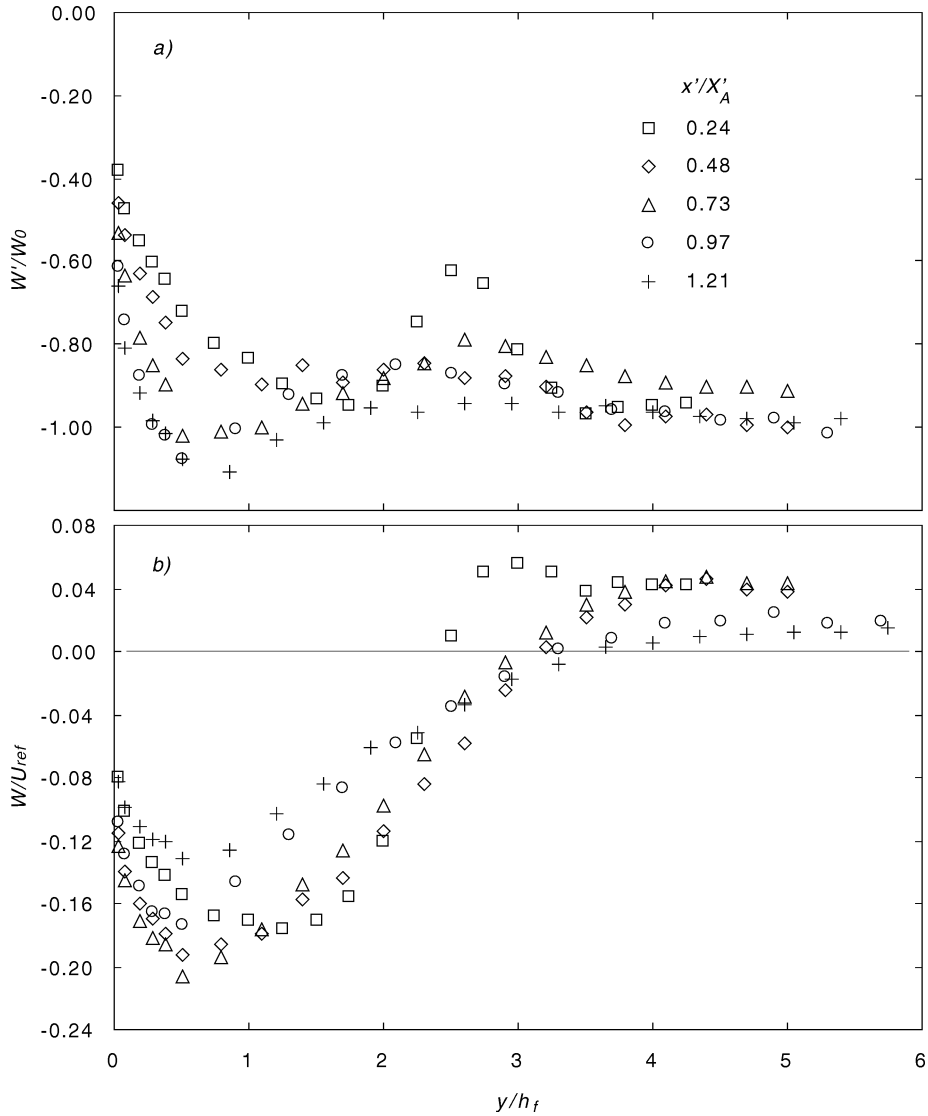

Figure 7. Cross-flow velocities W' and W against y, at $z = 380$ mm: (a) W'/W_0; (b) W/U_{ref}.

becomes positive (i.e. outward) before it subsequently reaches zero in the free stream. This is an inviscid effect which arises from the acceleration of U' above U_0. It was probably not noticed by McCluskey and Hancock because in their flow, unlike here, there was no plane of symmetry providing a check on probe alignment; the positive W in the *figure 8* amounts to a flow angle of less than 2.5°. The variation of W with U is not as simple as given Hancock and McCluskey, who found a clearly linear relationship between U and W, independent of x'/X'_A, outside the position of the negative peak. From similar plots (not included in this paper) at smaller z it appears that this is because the present flow is not as closely spanwise-invariant as was their flow. The independence they observed was therefore a consequence of spanwise invariance.

The effect of the viscous constraint on $W'(y)$ is clearly seen in *figure 7(a)*. The position at which the magnitude of $W'(y)$ has reached its maximum and the velocity at this position are defined as $\delta_{W'}$ and W'_δ, respectively, where these quantities represent the thickness of the near wall layer associated with the z'-direction

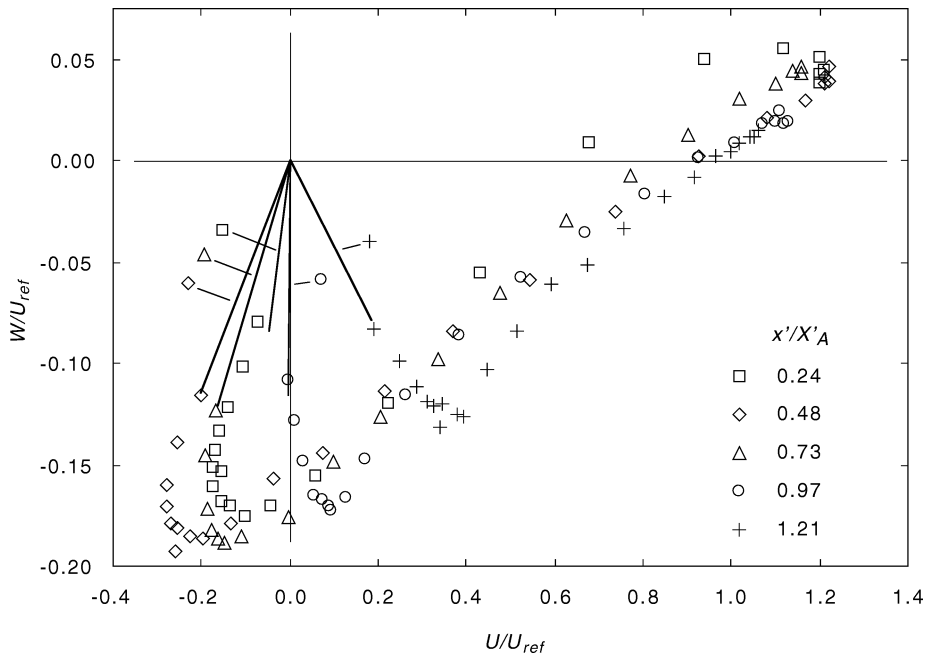

Figure 8. Polar plot of U against W, at $z = 380$ mm. Lines show the directions implied by the wall shear stress vector.

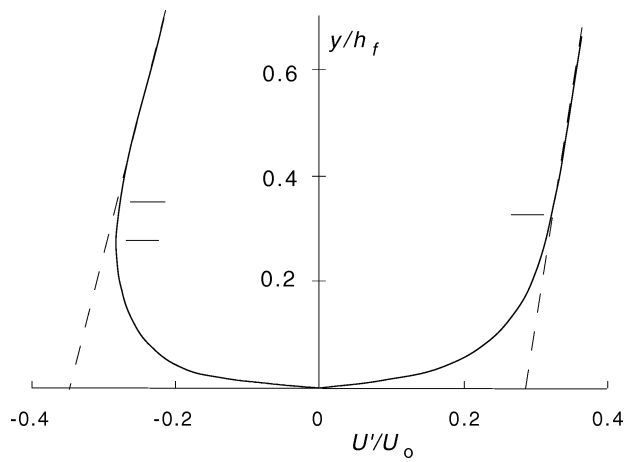

Figure 9. Illustration of near-wall velocity profile $U(y)$. Based on measurements at x'/X'_A of (a) 0.48 and (b) 1.2, $z = 380$ mm. Broken line is extrapolation of 'external' velocity gradient. Positions of layer edge, $\delta_{U'}$, indicated (see text).

flow and its 'external' velocity. The effect of the viscous constraint on $U'(y)$ behaves in a similar manner, except that U' continues to vary with y, because of the gradient that exists in the outer part of the flow, as illustrated in *figure 9*. The consistent definition for the x'-direction flow is to define the thickness, $\delta_{U'}$, as the point where the velocity gradient reaches the relatively constant level of the outer flow, and to define the external velocity, U'_δ, as that at the height $\delta_{U'}$. However, previous investigators have confined their attention to the reverse-flow region, and have defined $\delta_{U'}$ as the height at which the magnitude of the reverse-flow velocity is a maximum, and U'_δ, as the velocity at this height. As is obvious from *figure 9* viscous effects must extend further, and such a definition cannot be applied downstream of attachment. In this paper we have retained the latter definition

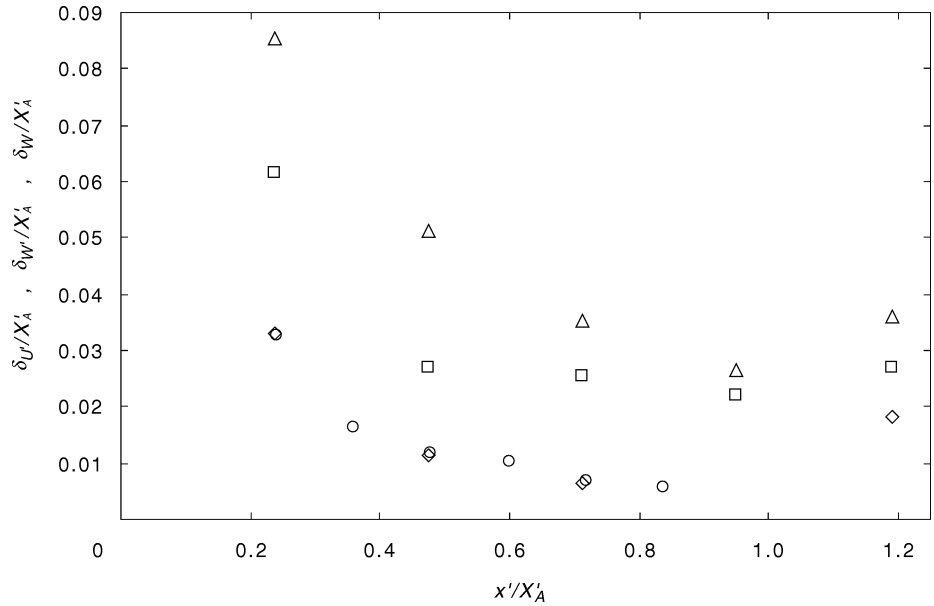

Figure 10. Thicknesses of near-wall layer, at $z = 380$ mm. ♢, $\delta_{U'}/X'_A$; ◯, ditto, unswept flow; △, $\delta_{W'}/X'_A$; □, δ_W/X'_A.

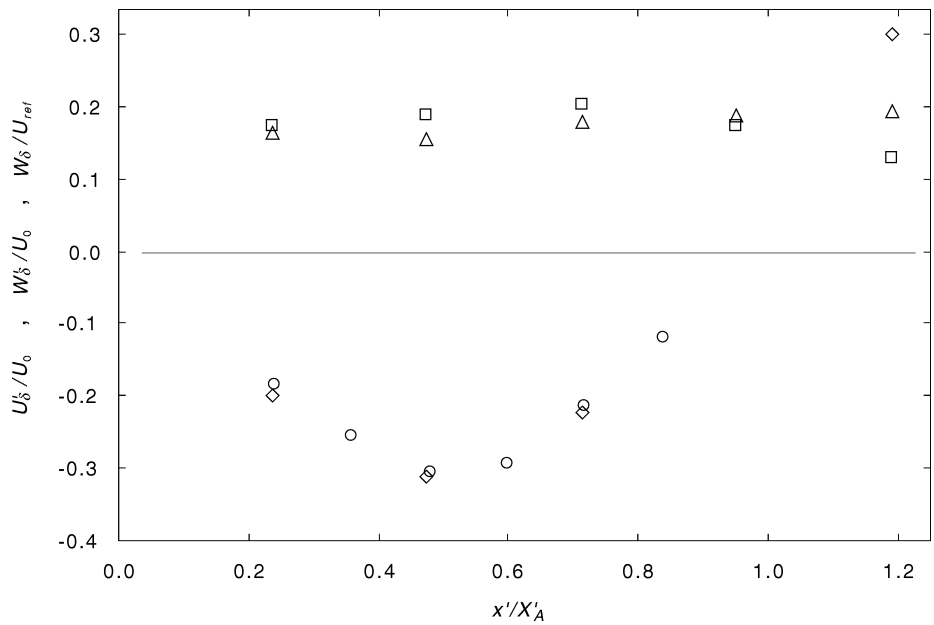

Figure 11. Velocities at edges of near-wall layer, at $z = 380$ mm. ♢, U'_δ/U_0; ◯, ditto, unswept flow; △, W'_δ/U_0; □, W_δ/U_{ref}.

upstream of attachment, though in the light of our results it is recommended that the former definition should be adopted in subsequent studies. The discrepancy in U'_δ, is very much smaller than that in $\delta_{U'}$, and negligible in the context here.

Clearly, it is not possible to determine the thicknesses very accurately from the present measurements because of the scatter in the relatively small velocity levels, though this limitation does not prevent gaining

some new ideas about the near-wall layer. Similar quantities can also be defined for $U(y)$ and $W(y)$, namely, δ_W and W_δ, and δ_U and U_δ. Here, the latter two are negligibly different from $\delta_{U'}$ and U'_δ, because of the low sweep angle. *Figure 10* shows the variation of these quantities with x'/X'_A, where $\delta_{U'}$ for the unswept flow is also given. (In addition, the comparability between $\delta_{U'}$ for the swept and unswept cases in *figure 10* is an indication of the repeatability of its measurement.) This figure summarises a feature, perhaps a surprising one, that is clearly notable from the profiles of U' and W', namely that $\delta_{W'}$ is substantially larger that $\delta_{U'}$. This is true even if the preferred definition of $\delta_{U'}$ discussed above is employed, where the discrepancy is largest at the stations $x'/X'_A = 0.48$ and 0.73, the preferred definition not exceeding that used by more than 30%. The difference is negligible at $x'/X'_A = 0.24$. The fact that the thickness, δ_W, is less than $\delta_{W'}$ is because W contains a contribution from U', but it is still significantly larger than δ_U. At the line of attachment, where $\tau_{x'}$ is by definition zero, $\delta_{U'}$ is not expected to be zero because the flow locally is a stagnation flow; the definition used here of the minimum in $U(y)$ would of course require it be zero, but the preferred definition would not, as the external gradient changes only slowly with x' (c.f. *figure 9*).

Although the effect of the no-slip condition reaches substantially further for the cross-flow than it does for the x'-direction flow, $\delta_{W'}$ is still markedly less than the height of the bubble, which at $x'/X'_A = 0.5$ is about $0.2X'_A$, for example, and, moreover, does not appear to be connected with a feature of the $U'(y)$-profile. As anticipated, the various thicknesses increase from a minimum at about the attachment position, perhaps a little earlier. The growth rate of $\delta_{U'}$ upstream of attachment would appear to be lower than it is downstream, consistent with favourable and adverse pressure gradients either side of attachment (*figure 5*). $\delta_{W'}$ and δ_W, on the other hand, grow about equally. Further towards the separation line, upstream of about $x'/X'_A = 0.4$, the growth rate of $\delta_{U'}$ increases as the pressure gradient changes sign. The growth rates of $\delta_{W'}$ and δ_W also increase, and near the separation line they become a substantial fraction of the bubble height. The edge velocities, W'_δ, W_δ, and U'_δ are shown in *figure 11*, where measurements for the unswept flow are again included. W'_δ, remains fairly constant, at about the free stream level, W_0. Clearly, U'_δ and W'_δ, behave very differently, as is to be expected.

The velocity profiles of the near-wall layers, namely U'/U'_δ and W'/W'_δ as functions of $y/\delta_{U'}$ and $y/\delta_{W'}$ are shown in *figures 12(a)* and *12(b)*. The first figure includes measurements from the unswept flow, which are seen to be no more than marginally different from the swept case. Though not shown here, both sets of measurements are close to those measured by previous investigators in unswept flow (Simpson, [3]; Adams and Johnston, [4]; Dianat and Castro, [5]; Devenport and Sutton, [6]), who have also found that the shape is virtually independent of position, x'/X'_A. The profiles of W'/W'_δ, shown in *figure 12(b)*, also show virtually no dependence on position, though as with those in *figure 12(a)* there is no obvious reason why they should behave in this way. The behaviour is remarkable, given the variation of the external flow with x'/X'_A. A further, distinctive feature is that the 'shapes' of U'/U'_δ and W'/W'_δ are also quite comparable, as shown in *figure 12(c)*. This is perhaps surprising in view of the fact that $\delta_{W'}$ is considerably larger than $\delta_{U'}$. The difference in shape is such that W'/W'_δ is slightly fuller near the surface and slightly less curved further out compared with U'/U'_δ. In shape, W'/W'_δ has some resemblance to that of a standard zero-pressure gradient turbulent boundary layer, and although there appears to be something of a logarithmic region the slope and intercept (inferred from the independently-measured wall shear stress) are roughly half the standard values.

Figure 13 shows the shear stress measurements of *figure 6* in the form of local coefficients, $\overline{C}_{f_{x'}}$ and $\overline{C}_{f_{z'}}$, defined as $\tau_{x'}/(\rho U'^2_\delta/2)$ and $\tau_{z'}/(\rho W'^2_\delta/2)$, as functions of local Reynolds numbers, $U'_\delta\delta_{U'}/\nu$ and $W'_\delta\delta_{W'}/\nu$, respectively. Streamwise positions are shown adjacent to the symbols. (This figure also includes data based on wind tunnel axes, which are discussed later.) $\overline{C}_{f_{x'}}$ and $\overline{C}_{f_{z'}}$ both behave in a comparable manner, though with one shifted with respect to the other. The line shown has a slope of -0.7. An exact similarity relationship between U'/U'_δ and $y/\delta_{U'}$ and between W'/W'_δ and $y/\delta_{W'}$ implies a slope of -1 in each case. The profiles cannot therefore be precisely self-similar, though presumably this cannot be seen here because any differences

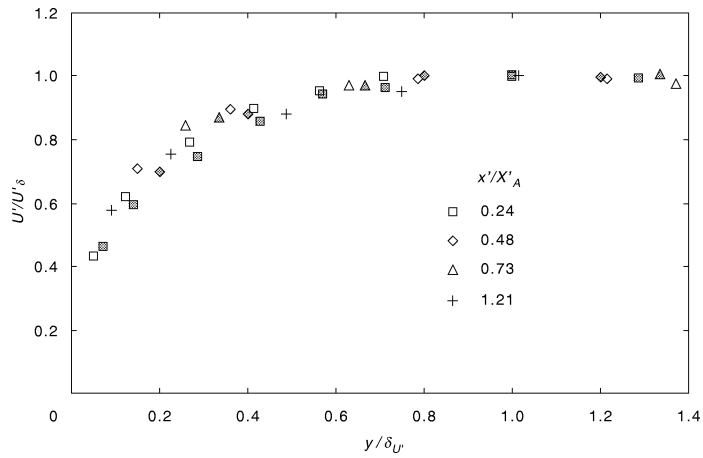

(a)

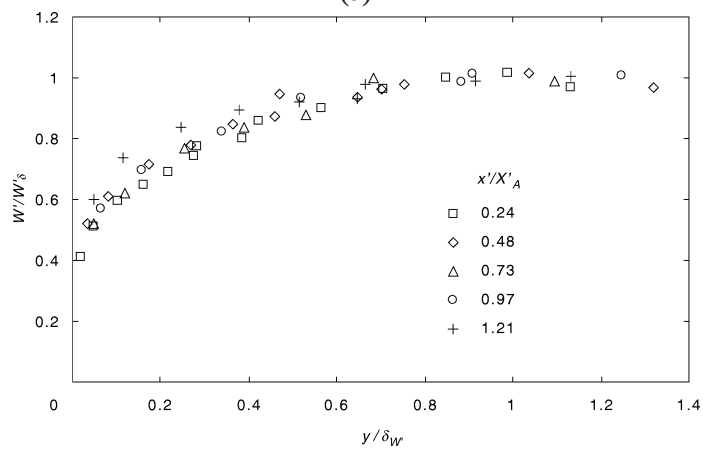

(b)

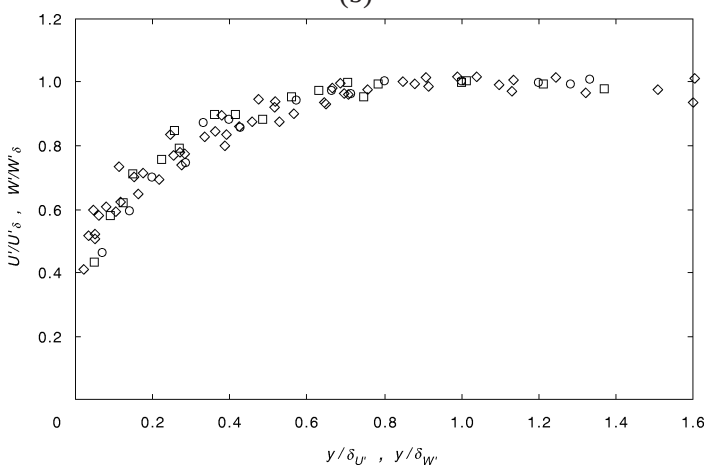

(c)

Figure 12. (a) Variation of U'/U'_δ with $y/\delta_{U'}$ in the near-wall layer, at $z = 380$ mm. Shaded symbols are unswept flow. (b) Variation of W'/W'_δ with $y/\delta_{W'}$ in the near-wall layer, at $z = 380$ mm. (c) Superposition of U'- and W'-profiles from (a) and (b). □, U'/U'_δ; ◯, U'/U'_δ, unswept flow; ◇, W'/W'_δ. All stations.

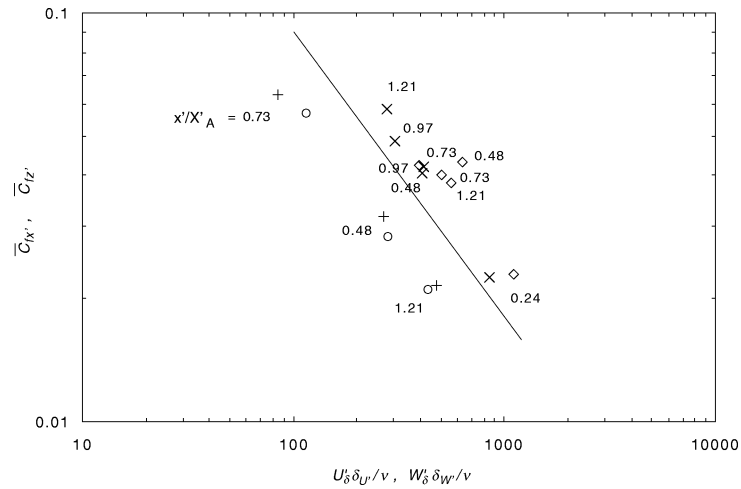

Figure 13. Local shear stress coefficients as a function of local Reynolds numbers ($z = 380$ mm). $x'-z'$ axes: $\circ\ \overline{C}_{f_{x'}}$ *versus* $U'_\delta\delta_{U'}/\nu$; $\diamond, \overline{C}_{fz'}$ *versus* $W'_\delta\delta_{W'}/\nu$. $x-z$ axes: $+, \overline{C}_{fx}$ *versus* $U_\delta\delta_U/\nu$; $\times, \overline{C}_{fz}$ *versus* $W_\delta\delta_W/\nu$. Line has slope of -0.7. Adjacent numbers show x'/X'_A.

are within the scatter. The slightly fuller profile shape of W'/W'_δ compared with U'/U'_δ noted earlier explains why $\overline{C}_{f_{z'}}$ is higher than $\overline{C}_{f_{x'}}$. (Were the Reynolds numbers above to be defined in terms of momentum thicknesses they would be about one tenth of those in *figure 13*, much smaller than that for turbulence to exist in a normal boundary layer.)

In a two-dimensional coplanar flow $\overline{C}_{f_{x'}}$ is a well-behaved simple function of the Reynolds number based on the distance from reattachment, $U'_\delta|X'_A - x'|/\nu$. In a spanwise-invariant, non-coplanar flow the distance along a surface streamline is again a unique function of the distance $X'_A - x'$, so it might be anticipated that $\overline{C}_{f_{x'}}$ and $\overline{C}_{f_{z'}}$ will exhibit well-behaved functions of $U'_\delta|X'_A - x'|/\nu$ and $W'_\delta|X'_A - x'|/\nu$. However, the behaviour is complex and quite different from that in the absence of cross flow. *Figure 13* therefore demonstrates a more general basis for the scaling of the near wall layer, though with a quantitatively distinct difference between that for $\overline{C}_{f_{x'}}$ and that for $\overline{C}_{f_{z'}}$. It should perhaps be mentioned that $\overline{C}_{f_{x'}}$ was not measured for the unswept flow though the implication of earlier comments is that its variation with $U'_\delta\delta_{U'}/\nu$ was as in *figure 13*. The present variation of $\overline{C}_{f_{x'}}$ with Reynolds number falls between that measured by Adams and Johnston [4] and that by Devenport and Sutton [6].

In summary, the near wall layer appears to be clearly governed by 'local'scaling based on U'_δ, $\delta_{U'}$, $W'\delta$ and $\delta_{W'}$, though with a quantitative difference between the x'- and z'-direction flows. Moreover, the present scaling applies equally upstream and downstream of attachment, and also appears to work through attachment. The fact that the flow is coplanar near the surface appears to be a consequence of the linear variations of U' and W' with y near the surface, and not some intrinsic relationship between U' and W'. U' increases more rapidly than W', approximately as the ratio $\delta_{W'}/\delta_{U'}$, of course, and the limit of coplanar behaviour must be somewhat less than $\delta_{U'}$.

While a spanwise-invariant flow clearly has an obvious axis system, the central converging flow does not. This is discussed further in the next section, but in preparation for that discussion it is helpful to consider the present case in wind tunnel axes. W/U_{ref} has already been presented in *figure 7(b)*. Although not shown here, the variation of W/W_δ with y/δ_W is indistinguishable from that of W'/W'_δ with $y/\delta_{W'}$ given in *figure 12(b)*, though given the comparison in *figure 12(c)*, this is not particularly surprising. *Figure 13* also shows the shear stress measurements but referred to wind tunnel axes, where the stresses τ_x and τ_z are normalised with respect to U_δ and W_δ, and the Reynolds number defined as $U_\delta\delta_U/\nu$ and $W_\delta\delta_W/\nu$. These shear stress coefficients exhibit

a comparable dependency on Reynolds number to that discussed above, though the implicit dependence on x is different for $\overline{C}_{f_z}$ near and downstream of attachment from that for $\overline{C}_{f_{z'}}$. On the other hand, because of the mild cross flow, $\overline{C}_{f_x}$ and $U_\delta \delta_U / \nu$ differ only slightly from $\overline{C}_{f_{x'}}$ and $U'_\delta \delta_{U'} / \nu$.

3.2. 'V-region' flow

All the measurements for this flow region will be presented in wind tunnel axes. A strictly more appropriate axis system might be one in which one axis (z'', say) is locally aligned along an isobar, and the other direction (x'', say) perpendicular to it. Such a system reduces to the $x'-z'$ axis system employed above in a spanwise-invariant flow. This $x''-z''$ system has not been tested against the present measurements, partly because of the task of defining the isobars accurately, and partly because of the near similarity observed earlier. Moreover, if

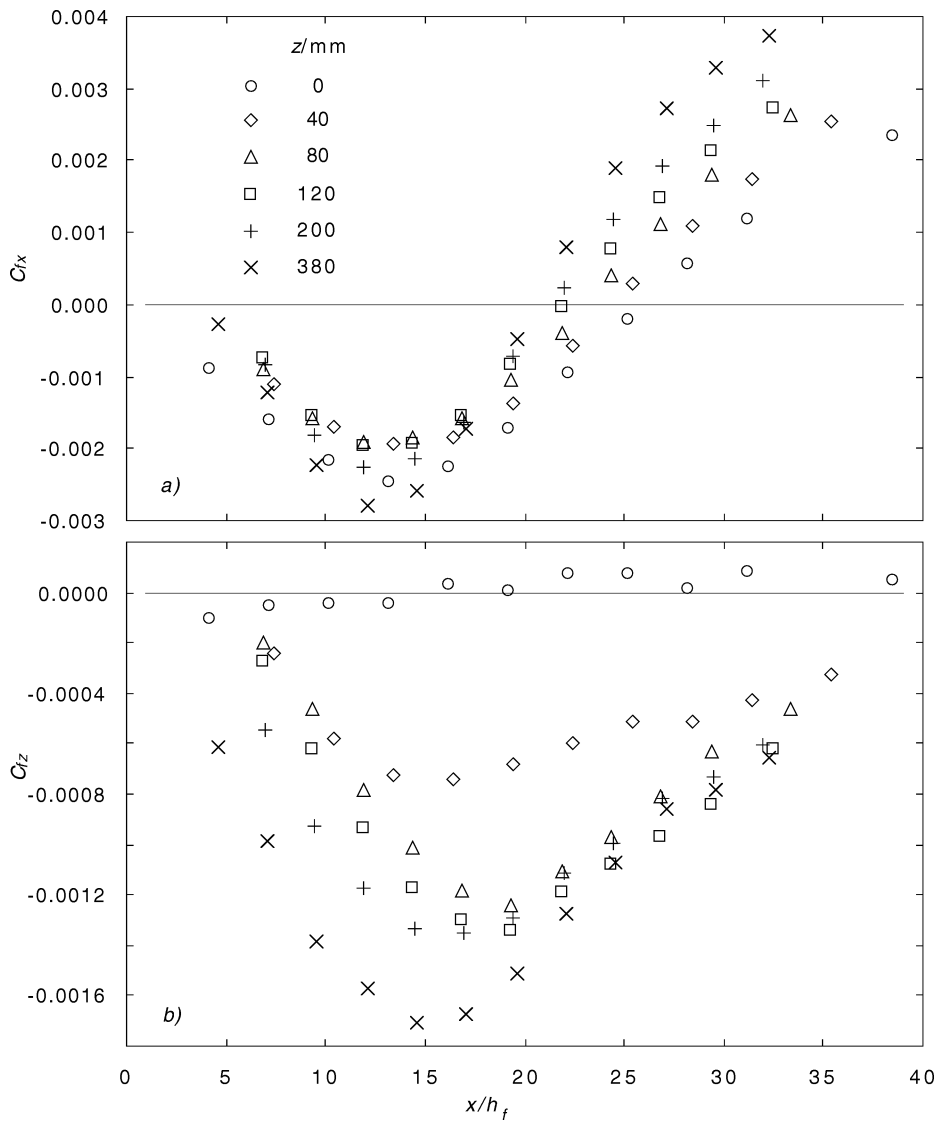

Figure 14. Shear stress coefficients in 'V-region': (a) C_{f_x}; (b) C_{f_z}. (Stresses normalised by U_{ref}.)

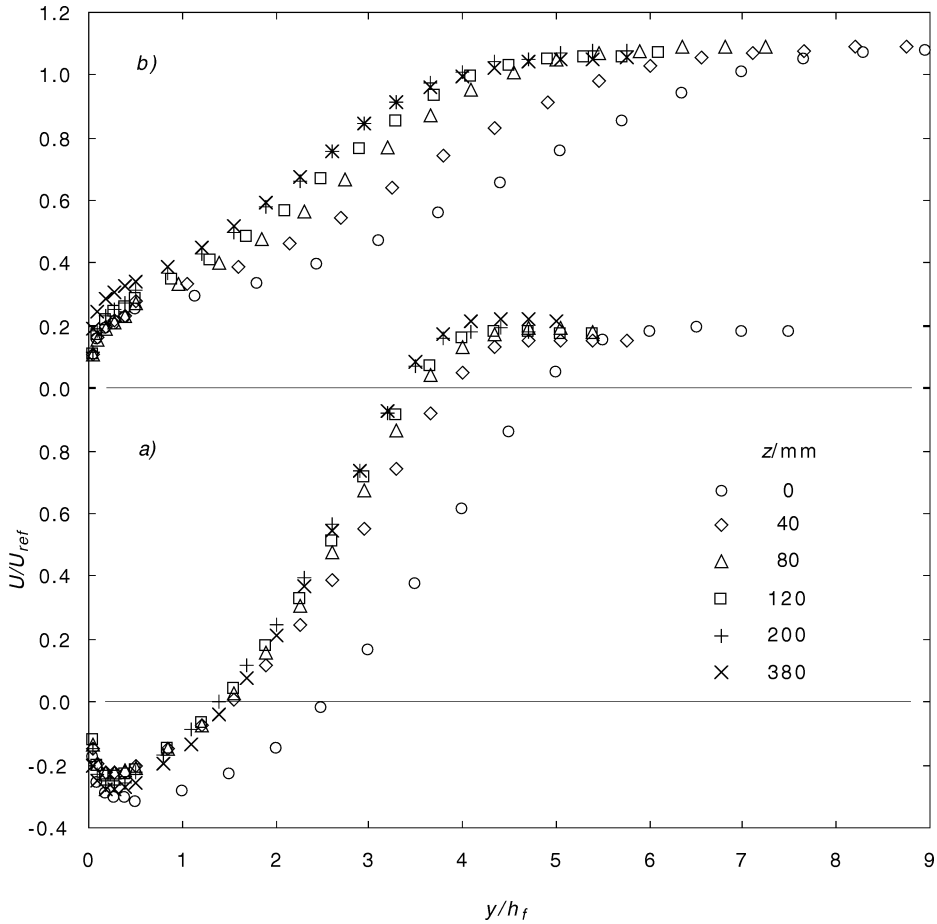

Figure 15. Profiles of $U(y)$, at (a) $x/X_A = 0.48$; (b) $x/X_A = 1.20$.

the flow in the central region behaves, when observed with respect to $x-z$ axes, in the same way as the flow in the spanwise-invariant region observed in $x'-z'$ axes, then it is likely that it will behave in much the same way if referred to $x''-z''$ axes.

Figure 14 shows C_{f_x} and C_{f_z} where the stresses τ_x and τ_z have been normalised by U_{ref}. A selection of profiles of U and W at x/X_A of 0.48 and 1.2 are shown in *figures 15* and *16*. The parameters δ_U, U_δ, δ_W and W_δ are now functions of z, but for reasons of space are not given here. The profiles of U/U_δ and W/W_δ as functions of y/δ_U and y/δ_W are shown in *figure 17*. Remarkably, within the limits imposed by the accuracy of the measurements, they each fall close to single curves, and if superimposed a similar comparison can be made to that given earlier. *Figure 18* shows shear stress coefficients, $\overline{C}_{f_x}$ and $\overline{C}_{f_z}$, against Reynolds numbers on the same basis as in *figure 13*, except that these are defined in terms of δ_U, U_δ etc. Data from *figure 13* is repeated in this figure. Clearly, at least to a reasonable approximation, $\overline{C}_{f_x}$ and $\overline{C}_{f_z}$ behave as in the spanwise-invariant case. Therefore, the local scaling observed previously also applies in this more general albeit mildly three-dimensional flow. If $\overline{C}_{f_x}$ and $\overline{C}_{f_z}$ are plotted against Reynolds numbers based on the distance $|X'_A - x'|$ instead of δ_U or δ_W, then the relationship is even more complex than that mentioned section 3.1.

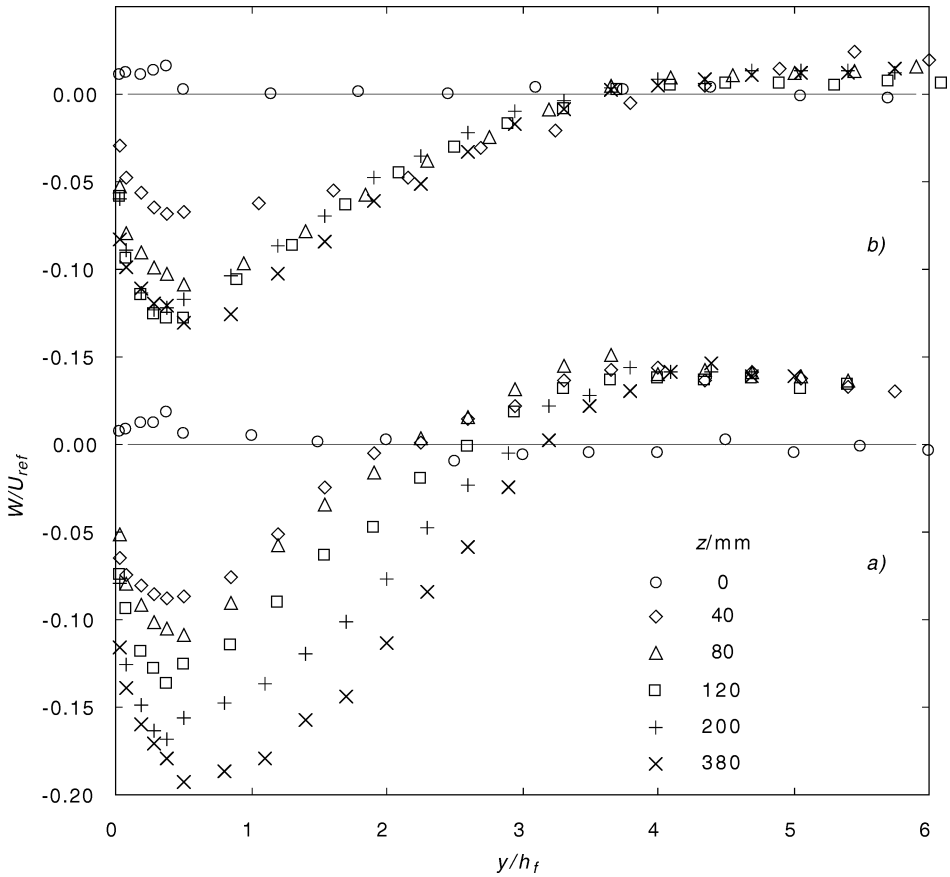

Figure 16. Profiles of $W(y)$, at (a) $x/X_A = 0.48$; (b) $x/X_A = 1.20$.

4. Further discussion

It might be anticipated that the near-wall layer should resemble a three-dimensional boundary layer with the reverse flow (in the x'- or x-directions) as the primary flow and the cross flow in the z'- or z-directions as the secondary flow. This would require δ'_W (or δ_W) to be less than $\delta_{U'}$, which evidently is not the case. There is however a clear resemblance which can be seen when the z'- or z-direction flow is thought of as the 'streamwise' flow of the ('3-d') boundary layer, and the x'- or x-direction flow is seen as the 'cross flow', driven primarily by the pressure gradient, $\partial p/\partial x'$. On the side upstream of attachment the 'cross flow' is towards the separation line, and on the side downstream of attachment the 'cross flow' is away from the separation line. The boundary layer studied by Anderson and Eaton [18] in which the cross flow was generated by a central wedge provides a useful qualitative illustration of diverging cross flow, except in their case the lateral pressure gradient was not like that here.

Viewed in this way, the effect of the viscous constraint extends to a much smaller distance for the x'-direction flow than for z'-direction flow, much as $\delta_{U'}$ is substantially less than $\delta_{W'}$ (*figure 10*). Indeed, the ratio $\delta_{U'}/\delta_{W'}$ is quantitatively comparable with the ratio of the height of the peak cross-flow velocity to the boundary layer thickness in a three-dimensional turbulent boundary layer, as can be seen from the measurements of Anderson and Eaton. What is more, the wall shear stresses are also quantitatively comparable once the boundary layer measurements are treated in the same way as here. This requires the lateral shear stress to be normalised by

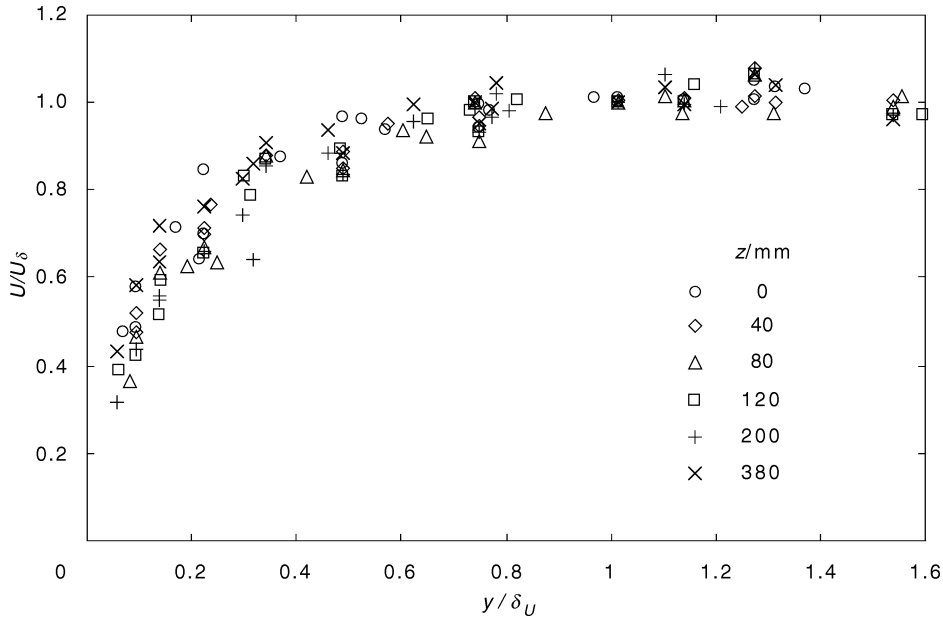

(a)

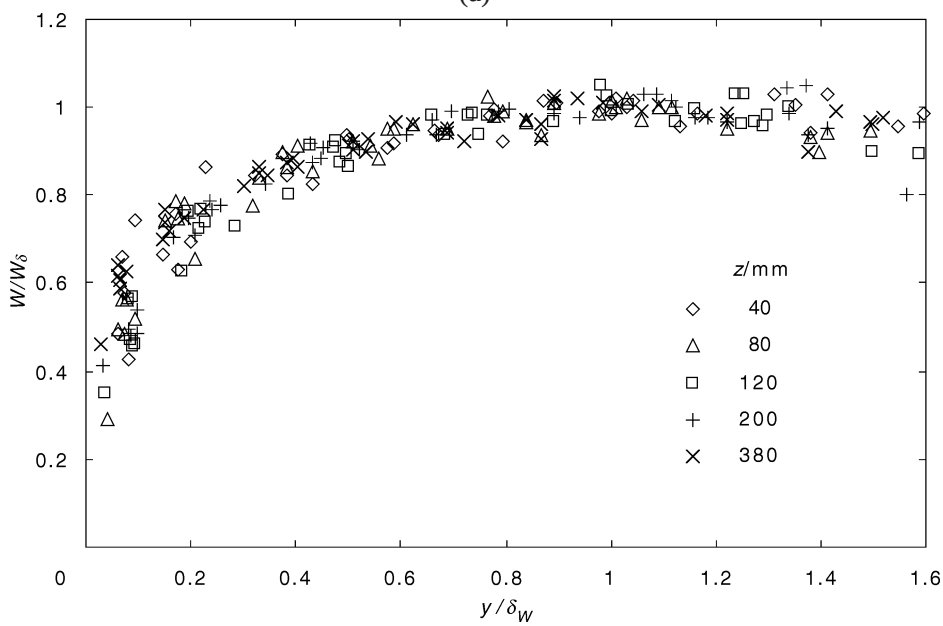

(b)

Figure 17. (a) Variation of $U(y)$ within the near-wall layer, all z-stations and $x/X_A = 0.24, 0.48, 0.73, 1.20$. (b) Variation of $W(y)$ within the near-wall layer, all x- and z-stations, except $z = 0$.

the peak in the cross-flow velocity and local Reynolds numbers to be defined as here (i.e. in terms of this peak velocity and the height it which it occurs, and the free-stream velocity and boundary layer thickness). The data of Bradshaw and Pontikos [19] is particularly useful for the comparison because the wall shear stress and direction have been measured independently of any assumption about the logarithmic law, which has been used

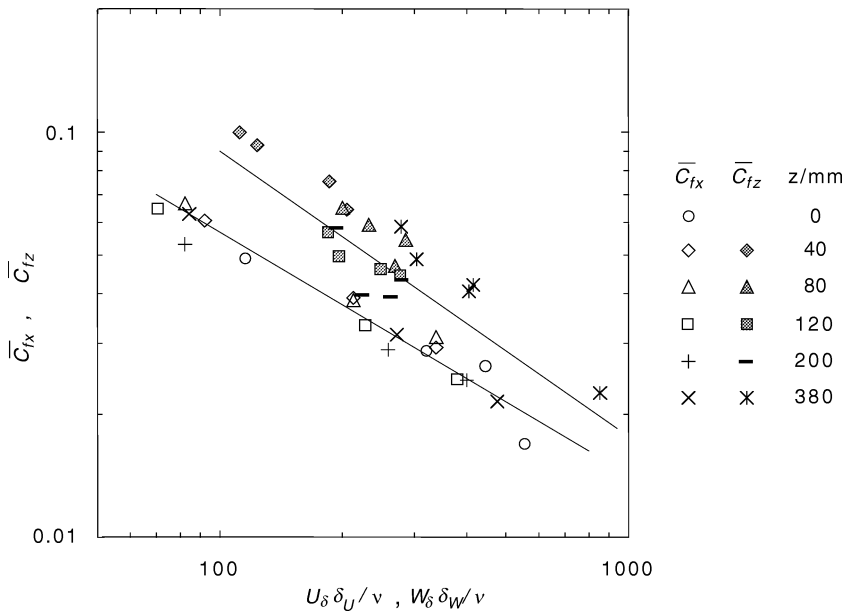

Figure 18. Local shear stress coefficients as a function of local Reynolds numbers. $x - z$ axes, all stations. Lines have slopes of -0.6 and -0.7.

in a number of studies to measure wall shear stress. Their case at $x = 1092$ cm, for example, transposed into the present axes, gives (from the cross-flow component) a $\overline{C}_{f_x}$ of 0.035 at a Reynolds number, $U_\delta \delta_U / \nu$, of roughly 500, and (from the streamwise component) a $\overline{C}_{f_z}$ of 0.0017 at a Reynolds number, $W_\delta \delta_W / \nu$, of about 79×10^3. The first is comparable with the data of *figure 18*, and although the latter coefficient and Reynolds number are, respectively, much smaller and much larger than in the present flow it is interesting to note that the implied dependence is comparable with that shown in *figures 13* and *18*, the values above implying a slope of -0.6.

The question remains as to why there is this seemingly workable transposition of directions. The fact that $\delta_{W'}$ is substantially larger than $\delta_{U'}$ together with the above discussion points to regarding the cross flow as the 'primary' feature of the near-wall layer, where in the special case of spanwise-invariant unswept flow the (time average of the) cross flow happens to be zero. In this framework the near-wall flow (in the spanwise-invariant case) deflected towards the separation line does not reverse, i.e. W' does not change sign. The deflection remains less than 90°, except in the limit of unswept flow when the deflection is instantly 90°. Increasing the sweep angle leads to a smaller deflection of the near-wall streamlines, decreasing the 'lateral' perturbation. In a three-dimensional boundary layer the peak in the cross-flow velocity appears always to fall within the inner layer, sometimes into the viscous sub-layer. From the present standpoint it is not surprising, therefore, that the reverse flow (the $-x$- or $-x'$-direction flow) behaves in a viscous-dominated manner. Further out, the direction changes from reverse flow to streamwise, corresponding to a change in sign of the cross flow in a three-dimensional boundary layer, as can happen when there is a change in sign of the lateral pressure gradient – see for example Bruns et al. [20] – though in the present flow this change is essentially stress driven. In overall terms, however, because a separated flow is considerably different from that of a three-dimensional boundary layer, it seems rather unlikely that there will be much more than a qualitative link, especially for turbulence quantities. Nevertheless, the present comparisons are striking, and further comparisons may prove useful.

5. Conclusions

Two flow types have been studied, namely the spanwise-invariant flow and a more general, mildly converging three-dimensional flow, with particular attention paid here to the near-wall layer. Reference has also been made to an unswept, two-dimensional, coplanar flow.

Contrary to what at first might be expected the viscous constraint on the cross flow velocity (z'-direction) extends substantially further into the flow than that on the 'streamwise' flow (x'-direction). The profiles of cross-flow velocity also exhibit an approximate self similarity, as previously observed for the streamwise flow in nominally two-dimensional coplanar flow, and demonstrated again here. Very near the surface the flow is, it seems, coplanar only in so far as the velocities vary linearly with y. Wall shear stress coefficients based on velocities at the edge of the respective near-wall layer exhibit simple dependencies on local Reynolds numbers based upon the edge velocities and layer thicknesses. These scalings apply either side of attachment, and also appear to apply through attachment. The distance from attachment is not a suitable scaling parameter in these more gereral flows.

There is a striking comparability between the near-wall flow and three-dimensional turbulent boundary layers. This requires the flow directions to be transposed from that which, prima facie, might be expected. That is, the cross flow is the primary flow, while the flow away from the attachment line is the secondary flow. On limited evidence the two are comparable quantitatively in that both exhibit comparable thickness ratios and comparable dependence of shear stress on Reynolds number. However, in overall terms, it seems likely that any comparison would be qualitative rather than quantitative, though even this would be helpful.

The measurements presented here were part of a study of the whole flow field. Further, locally more accurate measurements confined to the near-wall layer with higher levels of cross flow would be useful.

Acknowledgements

This work was part of that funded by EPSRC grant GR/H78689. Progress in the work here has undoubtedly benefited directly as a result of the long standing collaboration between Professor Hans Fernholz' group in Berlin and the group at Surrey, especially the collaborative work on the through-wall probe (Schober et al.) and for the invitation to PEH to work in Berlin. We are grateful too for the support given by our colleague Professor Ian Castro, and for his comments on a draft of this paper.

References

[1] Sutton E.P., Devenport W.J., Barkey Wolf F.D., Experimental studies of the reattachment of separated shear layers, in: Kozlov V.V., Dovgal (Eds), IUTAM Symp., Separated Flows and Jets, Springer-Verlag, 1990, pp. 573–588.
[2] Fernholz H.H., Janke G., Kalter M., Schober M., On the separated flow behind a swept backward-facing step. Physics of separated flows – numerical, experimental and theoretical aspects, Notes on Numerical Fluids Mechanics 40 (1993) 200–207.
[3] Simpson R.L., A model for the backflow mean velocity profile, AIAA J. 21 (1983) 142–143.
[4] Adams E.W., Johnston J.P., Flow structure in the near-wall zone of a turbulent separated flow, AIAA J. 26 (8) (1988) 932–939.
[5] Dianat M., Castro I.P., Measurements in separating boundary layers, AIAA J. 27 (1989) 719–724.
[6] Devenport W.J., Sutton E.P., Near-wall behaviour of separated and reattaching flows, AIAA J. 29 (1) (1991) 25–31.
[7] Hancock P.E., Low Reynolds number two-dimensional separated and reattaching turbulent shear flow, J. Fluid Mech. 410 (2000) 101–122.
[8] Hancock P.E., McCluskey F.M., Spanwise-invariant three-dimensional separated flow, J. Exp. Thermal Fluid Sci. 14 (1) (1997) 25–34.
[9] Hardman J.R., Hancock P.E., Moderately three-dimensional separated and reattaching turbulent flow, in: 2nd Int Symp. on Turbulence, Heat and Mass Transfer, Delft, June 1997, pp. 541–548.
[10] Johnston J.P., On the three-dimensional turbulent boundary layer generated by secondary flow, T. ASME D, J. Basic Eng. 82 (D) (1960) 233–248.
[11] Hardman J.R., Moderately three-dimensional separated and reattaching turbulent flow, PhD thesis, University of Surrey, 1998.

[12] Schober M., Hancock P.E., Siller H., Pulsed-wire anemometry near walls, Exp. Fluids 25 (1998) 151–159.
[13] Patel V.C., Calibration of the Preston tube and limitations on its use in pressure gradients, J. Fluid Mech. 23 (1965) 185–208.
[14] Langston L.S., Boyle M.T., A new surface flow-visualisation technique, J. Fluid Mech. 125 (1982) 53–57.
[15] Hancock P.E., Measurements of mean and fluctuating wall shear stress beneath spanwise-invariant separation bubbles, Exp. Fluids 27 (1999) 53–59.
[16] Ruderich R., Fernholz H.H., An experimental investigation of a turbulent shear flow with separation, reverse flow and reattachment, J. Fluid Mech. 163 (1986) 283–322.
[17] Castro I.P., Haque A., The structure of a turbulent shear layer bounding a separation region, J. Fluid Mech. 179 (1987) 439–468.
[18] Anderson S.D., Eaton J.K., Reynolds stress development in pressure-driven three-dimensional turbulent boundary layers, J. Fluid Mech. 202 (1989) 263–294.
[19] Bradshaw P., Pontikos N.S., Measurements in the turbulent boundary layer on an 'infinite' swept wing, J. Fluid Mech. 159 (1989) 105–130.
[20] Bruns J.M., Fernholz H.H., Monkewitz P.A., An experimental investigation of a three-dimensional turbulent boundary layer in an 'S'-shaped duct, J. Fluid Mech. 393 (1999) 175–213.